IEEE Access
Multidisciplinary | Rapid Review | Open Access Journal

Received January 7, 2016, accepted January 24, 2016, date of publication February 11, 2016, date of current version March 10, 2016.

Digital Object Identifier 10.1109/ACCESS.2016.2528822

Effects of Practical Rechargeability Constraints on Perpetual RF Harvesting Sensor Network Operation

DEEPAK MISHRA, (Student Member, IEEE), AND SWADES DE, (Senior Member, IEEE)
Department of Electrical Engineering, and Bharti School of Telecommunication, IIT Delhi, New Delhi, Delhi 110016, India

Corresponding author: S. De (swadesd@ee.iitd.ac.in)

This work was supported by the Department of Science and Technology under Grant SB/S3/EECE/0248/2014.

ABSTRACT Green perpetual sensor network operation is the need of the hour for critical applications, such as surveillance, military, and environment monitoring. Mobile integrated data collection and recharging is a promising approach to meet this requirement by routinely visiting the field nodes for collecting the sensed data and supplying energy via radio frequency (RF) energy transfer. Practical constraints, such as self-discharge and aging effects of the energy storage element (supercapacitor), significantly impact the renewable energy cycle (REC) and, hence, strongly influence the performance of RF energy harvesting networks. To account for the nonidealities in practical supercapacitors, in this paper, a circuit model for REC is proposed, and corresponding RF charging time and node lifetime expressions are derived. Hardware experiments are performed to validate the proposed REC model. REC for complicated supercapacitor models is characterized using duality principle and a generic simulation model. Using the developed analytical models for practical supercapacitors, the size of network for perpetual operation is estimated, which is demonstrated to be significantly less than that predicted by considering ideal supercapacitor behavior. For example, with three-branch supercapacitor model, the estimated sustainable network size is shown to be nearly 52% less than that offered by the ideal supercapacitor model.

INDEX TERMS Charging time characterization, integrated data collection and recharging, practical supercapacitor models, radio frequency energy transfer, renewable energy cycle.

I. INTRODUCTION

Wireless Sensor Networks (WSNs) have wide range of applications, such as, environment monitoring and surveillance [1], [2]. However, finite on-board energy of the senor nodes limits its widespread usage. Energy harvesting and wireless power transfer (WPT) offer the potential to green perpetual network operation. Radio frequency (RF) energy harvesting (RFEH) from ambient sources is such an energy refilling approach that addresses the carbon footprint concerns. Unlike the other harvesting techniques [3], RF energy transfer (RFET) from dedicated source(s) provides more controlled operation and enables energy sharing among rechargeable devices.

Efficient data collection from the field sensors is another important aspect in WSNs. Traditional methods suffer from two major problems. First, direct data transfer to a remote sink may consume excessive battery energy of field nodes due to super-linear path loss. Second, even if multi-hop techniques are adopted, the network may suffer from *hot-spot* problem [4], where the nodes closer to the sink deplete energy at a faster rate because of handling higher volume of relayed traffic. To this end, in mobility-assisted schemes [5], the mobile data collectors with controlled mobility visit the field nodes to collect data that saves energy and provide balanced energy depletion. To achieve uninterrupted network operation, we consider the existence of an optimal tour of a mobile robot which visits the field nodes routinely to collect the field data and replenish the drained energy via dedicated RFET. Extending the concept of conventional data mobile ubiquitous LAN extensions (MULE), such a mobile robot acts as an integrated data and energy MULE (iDEM) [6].

A. MOTIVATION

Integrated data collection and recharging using iDEM for perpetual network operation involves a renewable energy cycle (REC), where the amount of energy stored at a field node must be at least equal to the energy consumed during

discharge phase of the cycle. So, REC has two phases: a) *charging*, b) *discharging* (see Fig. 1). Charging is done via RFET from iDEM. Discharging phase involves drainage of the stored energy for carrying out various field node operations. To quantify the efficiency of iDEM-powered WSNs, recharging process as well as leakage of the node's energy storage element (supercapacitor) need to be characterized. Practical supercapacitor models are more complex than the ideal ones due to the nonidealities like self-discharge, leakage current, and aging effects. So, consideration of practical supercapacitor characteristics is very crucial in iDEM path planning for a realistic estimate of perpetual network operation.

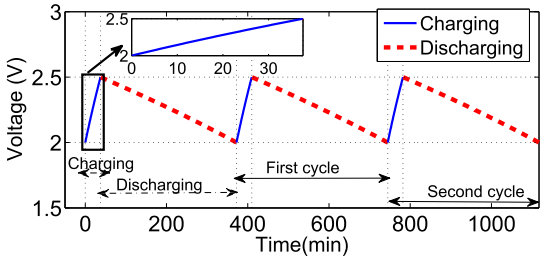

FIGURE 1. Renewable energy cycle. The charging and discharging cycles represent the voltage across the supercapacitor with capacity $C = 50$F, charging DC power $P = 25$mW, and loading power $P_{cons}^{avg} = 2.8$mW. This figure is plotted by using the equations for charging and discharging time derived later in Sections IV-Aand IV-B, respectively.

B. KEY CONTRIBUTIONS

Objective of this paper is to estimate the sustainable network size using iDEM, for perpetual operation of energy-hungry field sensor nodes that are operated by practical rechargeable supercapacitors. Key contributions of this work are as follows:

i) Practical REC circuit model is proposed along with its analytical characterization and experimental validation.
ii) Analytical RF charging time equations are developed for the practical supercapacitor models.
iii) Based on a novel duality principle, constant-power loading time of field nodes is characterized using RF charging equations. This behavior is experimentally validated.
iv) A reliable simulation model is developed that closely approximates the charging and loading behaviors of the analytically-intractable, practical supercapacitor models.
v) The developed loading models are used to estimate the node lifetime of practical wireless field sensor nodes.
vi) From the estimated (potentially random) node lifetime and RF charging time characteristics, sustainable network size supported by a single iDEM is obtained.

C. PAPER ORGANIZATION

Prior art is surveyed in Section II. The proposed REC circuit model and its role in perpetual network operation are discussed in Section III. Analytical characterization of RF charging time and duality principle establishing a relationship between constant-power charging and loading times are presented in Section IV. REC circuit model is experimentally validated in Section V. A generic simulation model is developed in Section VI for characterizing REC with advanced supercapacitor models. Sustainable network size supported by a single iDEM is evaluated in Section VII. Section VIII concludes the paper.

II. RELATED WORK

WIRELESS POWER TRANSFER

WPT can be classified in two main categories [7]: (i) non-radiative techniques which include inductive coupling and magnetic resonance coupling, and (ii) electromagnetic radiation based schemes which include RF waves, microwaves, and light waves. Periodic replenishment of the nodes' battery energy via non-radiative WPT was considered in [8]. The application of RFET for prolonging lifetime of rechargeable WSNs has been discussed in [6], [9]–[11].

Recently, there has been a growing attention towards improving RFET efficiency for realizing uninterrupted operation of WSNs [12]. With the advancement in RF harvesting circuit designs [13], smart cooperative energy sharing schemes [14], [15], and multi-antenna based energy beamforming technologies [16], the gains achieved from dedicated RFET have significantly increased. However for practical realization of perpetual WSN operation, hardware constraints involved in charging and discharging of RF-powered nodes needs to be accurately characterized [17].

CHARGING AND LOADING TIME CHARACTERIZATION

In a recent study [18], RFET has been shown to provide constant-power charging of the on-board supercapacitor. This work also developed RF charging equations for series RC circuit based supercapacitor model. The energy consumption models of wireless sensor node are provided in [19]–[21]. The studies in [22] and [23] assumed the field node to be a constant-power load that is powered by the energy stored in the supercapacitor. Constant-power loading equations for series RC circuit are provided in [24] and [25]. The simplified models developed in [18] and [22]–[25] provide valuable insights on charging and loading process. However, our experimental observations suggest that, practical supercapacitors require more elaborate considerations for accurate characterization of charging and loading process.

PRACTICAL SUPERCAPACITOR MODELS

Leakage and aging of the on-board supercapacitor are the two major practical aspects to be accounted, as they have significant impact on the energy harvesting network performance. In the existing works, supercapacitor has been modeled considering ideal capacitor [23], or series RC circuit [18], or a simplified equivalent circuit with series and parallel resistances to account the short-term leakage effects [26]. The non-ideal characteristics of supercapacitor

is due to its internal construction [26], which is different from that of a regular capacitor. Most popular supercapacitor model which accounts the long term behavior was presented in [27]. This model was extended in [28] to represent the behavior of supercapacitors at both low and high frequencies. An accurate modeling of dynamic diffusion phenomenon of supercapacitor residual charge during charging/discharging and rest phases was proposed in [29]. Although the prior works [23], [26]–[29] considered supercapacitor models with different degrees of complexity, analytical characterization of charging and loading times, required for energy harvesting network performance evaluation, is missing in the literature.

INTEGRATED DATA COLLECTION AND RECHARGING

Mobile platform for data collection and recharging was presented in [30] to minimize overall network energy consumption. Non-radiative energy transfer based joint optimization of effective charging and data collection was recently studied in [31]. In another non-radiative approach [32], network utility maximization problem under flow conservation, energy balance, and link capacity constraints was studied. The above works leave scopes on accounting varying energy consumption of the nodes [33] and dynamic data collection requirements [5], which would bring up additional challenges of on-demand iDEM service.

In the current work, we use radiative RFET because it does not have the strict constraints of distance, inter-node alignment or resonant coupling. Rather, it has the beam steering capability to enhance energy transfer gains [15] and provides simultaneous recharging of multiple nodes [17]. Also, it enables joint energy and field data transfer over the same RF signal.

III. PROPOSED CIRCUIT MODEL FOR REC CHARACTERIZATION IN PERPETUAL NETWORK OPERATION

A. RENEWABLE ENERGY CYCLE CIRCUIT MODEL

For perpetual network operation, remaining energy at each rechargeable node must follow a cycle, which is defined below:

Definition 1: Energy stored in the supercapacitor follows *renewable energy cycle (REC)* with period τ_{rec} if the energy consumption E_{cons} during τ_{rec} is at most equal to the energy stored E_{stored} in the supercapacitor at the beginning of the cycle, and thus the energy level never falls below the minimum required energy level E_{min}. E_{min} takes care of the energy required for sending the field node's data to the iDEM. Mathematically, $E_{cons} \leq E_{stored} = E_{supp} - E_{lost}$, where $E_{supp} = PT_C$ is the DC energy (P is the DC power, T_C is the charging time) available at the field node through RFET, and E_{lost} is the energy lost due to leakage and aging effects.

We present circuit models for REC characterization, as shown in Fig. 2, which comprise of constant-power charging and loading of practical supercapacitor models. In Fig. 2(a), the DC power P available after RF-to-DC conversion by

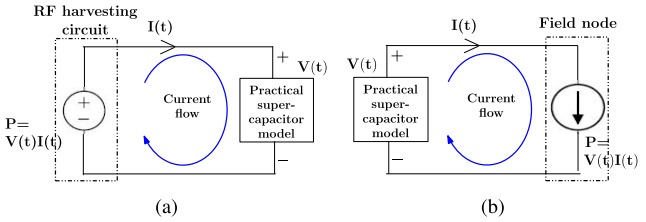

FIGURE 2. Proposed REC (charging + loading) circuit model. (a) Constant-power charging. (b) Constant-power loading.

P1110 IC [34] is modeled as *constant power source* with $V_{OUT} = V(t)$ as the source voltage and $I(t)$ as the source current [18]. In Fig. 2(b), a field node having DC-DC converter is modeled as a *constant-power load* operated by the energy stored in the supercapacitor, with $I(t)$ as the loading current.

B. ROLE OF REC IN PERPETUAL NETWORK OPERATION

Here we first discuss preliminaries of the application network considered, followed by the role of accurate REC characterization in analyzing the feasibility of its perpetual operation.

1) NETWORK MODEL

We have considered a pollution monitoring WSN with static field nodes $\mathcal{N}$ deployed in the field following Poisson point process. d_{ij} is the Euclidean distance between the nodes i and j ($i, j \in \mathcal{N}$). Each node consists of: a) one or more toxic gas sensors, b) memory card for data storage, c) low-power micro-controller, d) energy harvesting unit, e) communication module, f) passive wake-up radio module, and g) an on-board supercapacitor. We have used (i) Alphasense gas sensors [20] for sensing CO, H_2S, SO_2, and NO_2, which generate current proportional to the toxicity level; (ii) Powercast P1110 [34] for RFEH; and (iii) Mica2 mote for data processing, storage, and communicating with the iDEM.

2) STATE-DEPENDENT CONSUMPTIONS

Energy consumption of a field node depends on its operation states (Fig. 3(a)). It senses the pollutant(s) at a rate s_r (samples/day). The CPU is periodically activated from sleep state to store the sensed data. The sensing duty cycle is: $D_C = N_{s/n}\frac{s_r(t_r+t_w)}{t_d}$, where $N_{s/n}$, t_r, t_w are respectively the

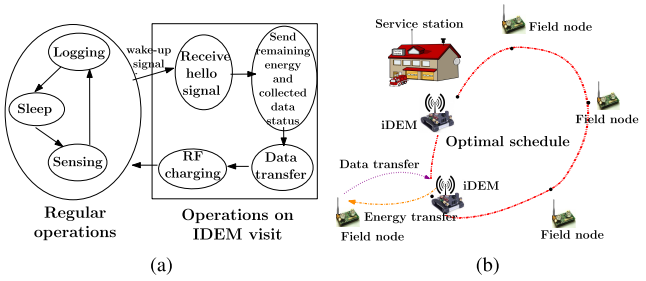

FIGURE 3. Application network model. (a) State diagram for node's operation. (b) iDEM scheduling.

number of sensors per node, sensor response time, and data logging time. Day duration $t_d = 86400$ sec. Upon arrival, the iDEM transmits a wake-up signal [35] to the field node. On receiving the wake-up signal, the node's CPU transits from sleep to active state and the radio switches to receive mode. Subsequently, on receiving a *"hello"* signal from iDEM, the node transits to transmit mode to send the status of remaining energy and collected data to the iDEM. This two-way handshake leads to data transmission, followed by RFET from the iDEM. For efficient WSN operation, we assume that the sensor node continues to perform its regular periodic operations (as mentioned in Fig. 3(a)) even during the RFET process because RF charging time may be high depending upon the capacitor size and node's remaining energy. Using the current consumption during different operation states at supply voltage $V_{op} = 3$ V and the time spent in each state, given in Table 1, the average power consumption $P_{cons}^{avg} = V_{op} I_{cons}^{avg}$ of a field node is calculated as:

$$P_{cons}^{avg} = \frac{3 \times t_d}{t_o + t_d}\left[\frac{D_C\,(t_r I_{se} + t_w I_w)}{t_r + t_w} + (1 - D_C)\, I_{sl}\right] + \frac{3 t_o I_o}{t_o + t_d} \tag{1}$$

where t_o and I_o are respectively the time spent and current consumption during communication and radio transition operation, which are performed only when the iDEM visits the node. I_{se}, I_w, and I_{sl} are current consumption during sensing, data logging, and sleep state.

TABLE 1. Current consumption in different states.

Operation		Current (A)	Time (s)
Sensing			
Toxic gas sensor	CO	657×10^{-3}	30
	SO_2	505×10^{-6}	40
	H_2S	547×10^{-6}	40
	NO_2	472×10^{-6}	50
Sensed data logging (Four bytes)			
CPU		8×10^{-3}	0.0518
ADC		1×10^{-3}	214.275×10^{-6}
Write		18.4×10^{-3}	0.0516
Sleep			
CPU		110×10^{-6}	Depends on duty cycle D_C
Memory		2×10^{-6}	
ADC		1×10^{-6}	
Radio		1×10^{-6}	
Sensing		110×10^{-6}	
Receive hello signal from iDEM (overhead [19] + data = 17 + 5 = 22 bytes)			
Initialize radio		6×10^{-3}	350×10^{-6}
Turn on radio		1×10^{-3}	1.5×10^{-3}
Switch to receive mode		15×10^{-3}	250×10^{-6}
Sample radio		15×10^{-3}	$350 \times 22 \times 10^{-6}$
Receive signal		15×10^{-3}	$416 \times 22 \times 10^{-6}$
Evaluate radio sample		6×10^{-3}	$100 \times 22 \times 10^{-6}$
CPU		8×10^{-3}	0.0082
Send Acknowledgment + Residual energy and collected data status + overhead = 26 bytes			
Switch to transmit mode		15×10^{-3}	250×10^{-6}
Transmit data		20×10^{-3}	$416 \times 26 \times 10^{-6}$
CPU		8×10^{-3}	0.0077

C. IDEM SCHEDULING AND IMPORTANCE OF REC

Given a renewable energy cycle along with a network model, *iDEM scheduling problem* is defined below:

Definition 2: Design an *optimal revisit schedule for the iDEM* so that it can serve the maximum number of nodes without letting the remaining energy of any node reduce below the threshold E_{min}, in minimum possible cycle time.

The iDEM starts from a service station (home) and is assumed to have sufficient energy to carry out its services before returning to home (cf. Fig. 3(c)). Depending on the energy consumption of a node, it may require multiple iDEM visits in a single period of schedule. The optimal iDEM schedule depends on iDEM revisit time at each node, which itself depends on three parameters[1]: a) RF charging time, b) loading time which is a function of P_{cons}^{avg}, and c) inter-node distances. As the inter-node distances are known and can be used to design the optimal schedule, our goal is to present analytical insights, backed by simulation and numerical results, on the charging and loading times for practical supercapacitor models.

IV. THEORETICAL ANALYSIS OF REC CIRCUIT MODEL

In this section we provide an analytical characterization of recharging cycle (or REC) for different supercapacitor models.

A. ANALYTICAL CHARACTERIZATION OF CHARGING TIME

First, we formally define RF charging time as follows:

Definition 3: RF charging time T_C is defined as the time required to charge a supercapacitor from some initial voltage $V_C = V_L$ to a fully-charged state with $V_C = V_H$.

As the voltage V_C across the supercapacitor is a function of time, we use V_C and $V_C(t)$ interchangeably without any difference in meaning. Now, we will derive the RF charging time equations for different supercapacitor models.

1) IDEAL MODEL

Here, supercapacitor is treated as a conventional capacitor. From Fig. 4(a), $P = V(t) \cdot I(t) = \frac{q}{C} \cdot \frac{dq}{dt}$. Using $q = CV_C$ and solving for V_C we obtain voltage $V_C(t)$ across an initially uncharged supercapacitor at any time t,

$$\int_0^{V_C} V_C dV_C = \int_0^t \frac{P}{C} dt \quad \text{or,} \quad V_C(t) = \sqrt{\frac{2Pt}{C}}. \tag{2}$$

From (2), current variation with time is obtained as $I(t) = \sqrt{\frac{PC}{2t}}$. RF charging time T_C^{ideal} for storing Q Coulombs of charge $\left(\text{or } V_C(t = T_C^{ideal}) \triangleq V_H\right)$ across an initially-uncharged supercapacitor $(V_C(t = 0) \triangleq V_L = 0$ V) is given by:

$$T_C^{ideal}(V_H) = \frac{C}{P}\int_0^{V_H} V_C dV_C = \frac{CV_H^2}{2P}. \tag{3}$$

[1]Data collection time is neglected, as it is very small [5] compared to RF charging time and also the field nodes are equipped with enough memory capacity for storing data over reasonably-long iDEM revisit interval.

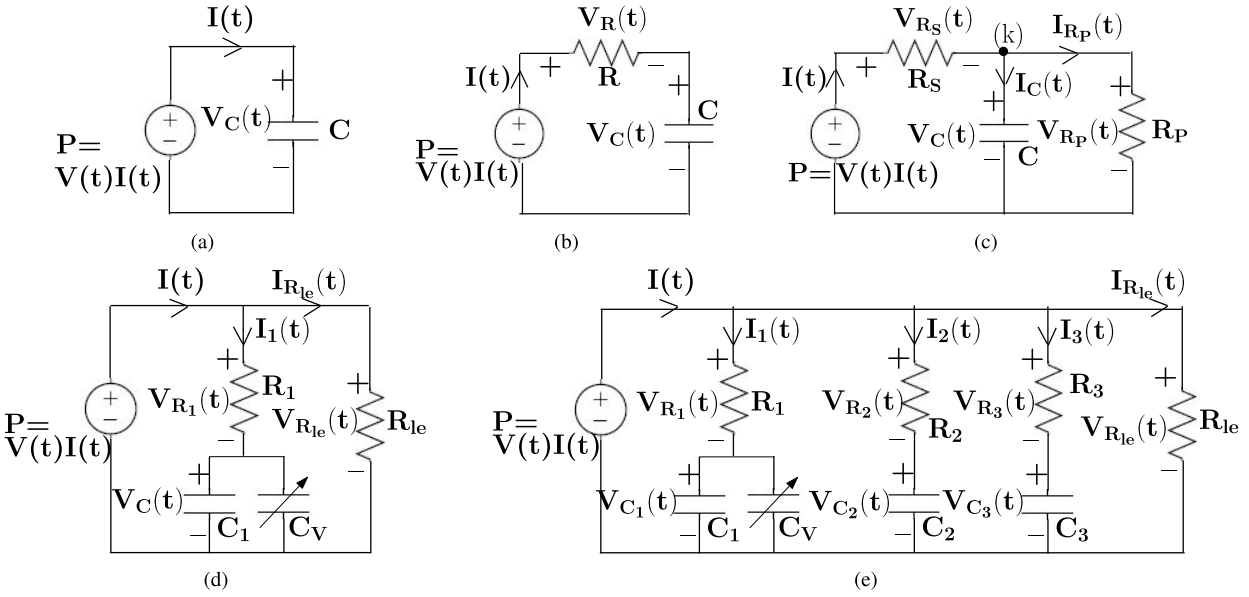

FIGURE 4. Supercapacitor models. (a) Ideal model [23]. (b) Commercial model [18]. (c) Simplified model [26]. (d) 1-branch model [27]. (e) Practical 3-branch model [27].

2) COMMERCIAL MODEL

This is the most commonly used and commercially adopted model of the supercapacitor which consists of a capacitor with an equivalent series resistance (ESR) R. Applying Kirchhoff's voltage law (KVL) in Fig. 4(b) we have, $P = V(t)\cdot I(t) = \left[V_R(t) + V_C(t)\right]\cdot I(t) = R\cdot\left(\frac{dq}{dt}\right)^2 + \frac{q}{C}\cdot\frac{dq}{dt}$. Substituting $q = CV_C$ and solving the resultant quadratic equation in $\frac{dV_C}{dt}$ to find the time T_C^{com} to charge an initially uncharged ($V_L = 0$) supercapacitor to voltage V_H, we obtain,

$$T_C^{com} = \frac{RC}{2}\left[\frac{2V_H}{\sqrt{V_H^2+4RP}-V_H} + \ln\left(\frac{\sqrt{V_H^2+4RP}+V_H}{\sqrt{V_H^2+4RP}-V_H}\right)\right] \tag{4}$$

The voltage across the capacitor at time t is:

$$V_C(t) = \frac{2\sqrt{RP}\left(1-\frac{1}{Z}\right)}{\sqrt{1-\left(1-\frac{1}{Z}\right)^2}},\quad \text{with } Z = \frac{1}{2}\left[1+W_0\left(e^{1+\frac{2t}{RC}}\right)\right] \tag{5}$$

where $W_0(\cdot)$ is the Lambert function (principal branch) [18]. The current across capacitor at time t is given as:

$$I(t) = C\frac{dV_C}{dt} = \frac{-V_C(t)+\sqrt{\left[\left(V_C(t)\right)^2+4RP\right]}}{2R}. \tag{6}$$

3) SIMPLIFIED MODEL

It consists of a capacitor with an ESR R_S and an equivalent parallel resistance (EPR) R_P and accounts for the short-term leakage effects. Applying KVL in Fig. 4(c),

$$P = V(t)\cdot I(t) = \left[I(t)\cdot R_S + I_{R_P}(t)\cdot R_P\right]\cdot I(t). \tag{7}$$

$I(t)$ in terms of $V_C(t)$ is obtained using Kirchhoff's current law (KCL) at node (k) in Fig. 4(c) as: $I(t) = \frac{V_C(t)}{R_P} + C\frac{dV_C(t)}{dt}$. Substituting in (7) gives $P = \left(\frac{V_C}{R_P}+C\frac{dV_C}{dt}\right)^2 R_S + V_C\left(\frac{V_C}{R_P}+C\frac{dV_C}{dt}\right)$, quadratic in $\left(\frac{V_C}{R_P}+C\frac{dV_C}{dt}\right)$, with solution:

$$\frac{V_C}{R_P} + C\frac{dV_C}{dt} = \frac{-V_C+\sqrt{\left[V_C^2+4R_SP\right]}}{2R_S}. \tag{8}$$

Solving (8) to find time T_C^{simp} required to charge an initially uncharged ($V_L = 0$) supercapacitor to voltage V_H, we obtain,

$$T_C^{simp} = \frac{R_PC}{4(R_P+R_S)}\left[R_P\ln\left(\frac{4R_SP}{\left(\sqrt{V_H^2+4R_SP}+V_H\right)^2}\right) + (R_P+2R_S)\ln\left(\frac{R_P^2P}{\left(R_P^2P-V_H^2(R_P+R_S)\right)}\right) + 2(R_P+2R_S)\tanh^{-1}\left(\frac{V_H(R_P+2R_S)}{R_P\sqrt{V_H^2+4R_SP}}\right)\right]. \tag{9}$$

Intuitively, T_C^{simp} is a function of V_L and V_H.

Similarly, by using $\frac{dI_{R_P}}{dt} = \frac{1}{R_PC}\left(I(t)-I_{R_P}(t)\right)$ and solving (7) for $I(t)$, the time $T_{C_I}^{simp}$ during which charging current

$$T_C^{pr_{1b}} = \frac{1}{4}\left\{2C_vR_{le}\left(2\sqrt{Y}-\sqrt{4Y+V_H^2}\right)-2C_vV_H(2R_1+R_{le})+C_1(2R_1+R_{le})\ln\left[\frac{PR_{le}}{\left(PR_{le}-V_H^2\right)}\right]\right.$$
$$+(2R_1+R_{le})\left[\left(\ln\left[\frac{\left(4\sqrt{PR_{le}}R_1(R_1+R_{le})+2R_{le}(2R_1+R_{le})\sqrt{Y}\right)\left(\sqrt{PR_{le}}+V_H\right)}{R_{le}\left(2R_1\sqrt{4Y+V_H^2}+R_{le}\left(\sqrt{4Y+V_H^2}-V_H\right)\right)+4\sqrt{PR_{le}}R_1(R_1+R_{le})}\right]\right)$$
$$\times\left(C_1-C_v\sqrt{PR_{le}}\right)+\left(\ln\left[\frac{R_{le}\left(2R_1\sqrt{4Y+V_H^2}+R_{le}\left(\sqrt{4Y+V_H^2}+V_H\right)\right)+4\sqrt{PR_{le}}R_1(R_1+R_{le})}{\left(4\sqrt{PR_{le}}R_1(R_1+R_{le})+2R_{le}(2R_1+R_{le})\sqrt{Y}\right)\left(\sqrt{PR_{le}}-V_H\right)}\right]\right)$$
$$\left.\times\left(C_1+C_v\sqrt{PR_{le}}\right)+C_v\sqrt{PR_{le}}\left(2\tanh^{-1}\left[\frac{V_H}{\sqrt{PR_{le}}}\right]+\ln\left[PR_{le}\right]\right)\right]+C_1R_{le}\ln\left[\frac{4Y}{\left(\sqrt{4Y+V_H^2}+V_H\right)^2}\right]\right\}. \quad (13)$$

$I(t)$ falls $I_H = I(t=0) = \sqrt{\frac{P}{R_S}}$ to $I_L = I\left(T_{C_I}^{simp}\right)$, is:

$$T_{C_I}^{simp} = R_PC\left[\frac{(R_P+2R_S)\ln\left[\frac{PR_P}{R_S\left(I_L^2(R_P+R_S)-P\right)}\right]}{2(R_P+R_S)}\right.$$
$$\left.-\ln\left(\frac{1}{I_L}\sqrt{\frac{P}{R_S}}\right)\right]. \quad (10)$$

4) PRACTICAL 1-BRANCH MODEL

To reflect the voltage dependence of capacitance, this model consists of a voltage-dependent differential capacitor comprising a fixed capacitance C_1 with parallel voltage-dependent capacitance C_v. Apart from series resistance R_1, a leakage resistor R_{le}, parallel to differential capacitor, is added to represent self discharge property. Applying KVL in Fig. 4(d),

$$V(t)=V_{R_1}(t)+V_C(t)=\left(\left[C_1+C_vV_C(t)\right]\frac{dV_C}{dt}\right)R_1+V_C(t). \quad (11)$$

Using $P = V(t)\left(\frac{V_{R_1}(t)}{R_1}+\frac{V_{R_1}(t)+V_C(t)}{R_{le}}\right)$ in (11) gives:

$$\left[C_1+C_vV_C\right]\frac{dV_C}{dt} = \frac{-V_C\left(1+\frac{2R_1}{R_{le}}\right)}{2\left[R_1+\frac{R_1^2}{R_{le}}\right]}$$
$$+\frac{\sqrt{\left[\left[V_C\left(1+\frac{2R_1}{R_{le}}\right)\right]^2+4\left(P-\frac{V_C^2}{R_{le}}\right)\left[R_1+\frac{R_1^2}{R_{le}}\right]\right]}}{2\left[R_1+\frac{R_1^2}{R_{le}}\right]}. \quad (12)$$

Solving (12), the time $T_C^{pr_{1b}}$ required to charge an initially uncharged supercapacitor ($V_L = 0$) to maximum voltage V_H, is given by (13), as shown at the top of this page. where $Y = \frac{PR_1(R_1+R_{le})}{R_{le}}$.

Note that, (13) is quite complicated, which hints analytical intractability of more realistic models. Temporal variation of charging current is given in Appendix A.

5) PRACTICAL 3-BRANCH MODEL

This is the most comprehensive model [27], that provides the desired insight into the complex terminal behavior of the supercapacitor. To account for the long-term behavior, apart from parallel leakage resistance R_{le}, it consists of three branches: a) first or immediate branch, with differential capacitor (fixed capacitance C_1 with parallel voltage-dependent capacitance C_v) and series resistance R_1, dominates immediate behavior of the supercapacitor in the range of seconds in response to a charge action; b) second or delayed branch has capacitance C_2 in series with resistance R_2, that dominates the terminal behavior in the range of minutes; c) third or long-term branch has capacitance C_3 in series with resistance R_3, determining the behavior for times longer than 10 min. Applying KCL in Fig. 4(e),

$$I_j(t)=\left[V(t)-V_{C_j}(t)\right]G_j\ \forall j\in\{1,2,3\},\ I_{R_{le}}(t)=V(t)G_{le} \quad (14)$$

Using (14) and $I(t) = \sum_{j=1}^{3} I_j(t) + I_{R_{le}}(t)$, we obtain:

$$P = (V(t))^2\left[\sum_{j=1}^{3}G_j+G_{le}\right]-V(t)\left[\sum_{j=1}^{3}V_{C_j}(t)G_j\right]. \quad (15)$$

(15) is quadratic with $V(t)$ as the unknown. Its solution is:

$$V(t) = \frac{1}{2\left(\sum_{j=1}^{3}G_j+G_{le}\right)}\left[\sum_{j=1}^{3}G_jV_{C_j}(t)\right.$$
$$\left.+\sqrt{4P\left(\sum_{j=1}^{3}G_j+G_{le}\right)+\left(\sum_{j=1}^{3}G_jV_{C_j}(t)\right)^2}\right] \quad (16)$$

where G_1, G_2, G_3, and G_{le} are the conductances, given by, $G_j = \frac{1}{R_j}\forall j \in \{1,2,3\}$, and $G_{le} = \frac{1}{R_{le}}$. Using (14) and (16), the state-space equations representing the behavior of variation of voltage across capacitors in different branches are given as:

$$\left[C_1+C_v\cdot V_{C_1}(t)\right]\frac{dV_{C_1}(t)}{dt}$$

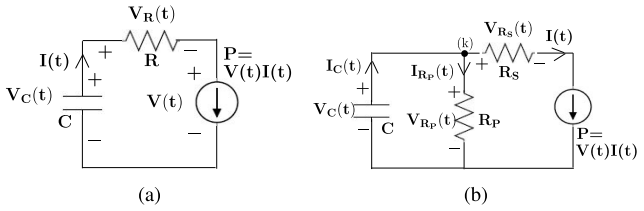

FIGURE 5. Analytical model for constant-power loading (CPL). (a) CPL of commercial model. (b) CPL of simplified model.

$$= \left[V(t) - V_{C_1}(t)\right] G_1 \tag{17}$$

$$C_j \frac{dV_{C_j}(t)}{dt} = \left[V(t) - V_{C_j}(t)\right] G_j, \quad \forall j \in \{2, 3\}. \tag{18}$$

$V(t)$ in (17) and (18) is a function of $V_{C_1}(t)$, $V_{C_2}(t)$, and $V_{C_3}(t)$, as given in (16). The given system of state-space equations is quite complicated and contains nonlinear terms, due to which it cannot be solved analytically. Moreover, further complex supercapacitor models have been proposed recently [28], [29], which are even more complicated and advanced than the above-discussed 3-branch model. To address these upcoming models, for which explicit analytical RF charging equations cannot be derived, we propose an generic and versatile simulation model in Section VI.

B. ANALYTICAL CHARACTERIZATION OF NODE LIFETIME

Lifetime of a node is defined as follows:

Definition 4: Lifetime T_{life} of a node is the time for which it can carry out its operation from the energy stored in its supercapacitor, or in other words, the remaining energy level for $t > T_{\text{life}}$ falls below E_{min} and the node lifetime expires.

So, for continuous operation of the field node, iDEM revisit time should be less than T_{life}. As mentioned in Section III-A, the DC-DC converter provides constant voltage to the load circuitry (i.e., the field node comprising of a processor and sensing circuits). So, as the voltage across the supercapacitor decreases with drained energy, the current consumption increases to maintain a constant voltage level for the node's proper operation. Thus, the wireless field node acts as a constant-power load. It may be noted that, due to high efficiency ξ_{DC-DC} of DC-DC converters in commercial motes (e.g., $\xi_{DC-DC} > 90\%$ in [36]), we assume that the power P drawn by the sensor node is equal to its actual average consumption P_{cons}^{avg}. However, in general $P = \frac{P_{cons}^{avg}}{\xi_{DC-DC}}$. Before we present a novel duality principle that will be used for deriving constant-power loading (CPL) time expressions, we define loading time and provide its relationship with T_{life}.

Definition 5: Loading time T_L is the time interval during which the voltage across a fully charged capacitor drops from V_H to V_L. If V_L corresponds to the minimum-required energy E_{min} in field node for its continued operation, then $T_{\text{life}} = T_L$.

1) DUALITY PRINCIPLE

Here we investigate an interesting relationship between the RF (or constant-power) charging and CPL time, that can be noted from Fig. 4(b) (or 4(c)) and Fig. 5(a) (or 5(b)). In particular, we demonstrate a duality relationship between the time required to charge a supercapacitor with capacitance C from an initial voltage V_L to a threshold voltage V_H using RF charging and the time required to discharge the supercapacitor from V_H to V_L using a constant-power load. Duality can be explained with the help of Figs. 2(a) and 2(b), where it is shown that the RF charging and constant power loading have a reciprocal relationship:

- The direction of current and power flow with respect to the supercapacitor are reversed (cf. Figs. 2(a) and 2(b)).
- The initial and final voltage/current levels are opposite.

Theorem 1: Duality principle implies that T_L *can be obtained from* T_C*, and vice versa, by applying following rules:*

$$\begin{aligned} \textit{Charging time } T_C &\longleftrightarrow \textit{Loading time } T_L; \\ P &\longleftrightarrow -P; \\ V_L \textit{ to } V_H \textit{ or, } I_H \textit{ to } I_L &\longleftrightarrow V_H \textit{ to } V_L \textit{ or, } I_L \textit{ to } I_H. \end{aligned} \tag{19}$$

Proof: Duality can be proved by first deriving CPL time expression for any supercapacitor model (without loss of generality) and then showing how applying duality rules to it gives the corresponding RF charging time equation derived in Section IV-A. We derive T_L expression for commercial model. On applying KVL and using $P = V(t) \cdot I(t)$ in Fig. 5(a),

$$P = \left[V_C(t) - V_R(t)\right] I(t) = -CV_C \frac{dV_C}{dt} - RC^2 \left(\frac{dV_C}{dt}\right)^2. \tag{20}$$

The solution of (20) is: $\frac{dV_C}{dt} = \frac{V_C - \sqrt{(V_C^2 - 4RP)}}{2RC}$. Solving for the loading time $t = T_L^{com}$, after which a fully-charged supercapacitor (with $V_C(t = 0) = V_H$) is drained to $V_C(T_L^{com}) = V_L$ (corresponding to E_{min}), we obtain:

$$\begin{aligned} T_L^{com} &= T_{load}^{com}(V_L) - T_{load}^{com}(V_H), \quad \text{with} \\ T_{load}^{com}(V_C) &= C \left[\frac{4RP\left[\ln\left(\hat{A}\right)\right] - V_C\hat{A}}{4P}\right] \end{aligned} \tag{21}$$

where $\hat{A} = \left(\sqrt{V_C^2 - 4RP} + V_C\right)$. Note that, (21) providing T_L^{com} as a function of V_L and V_H is valid only for $V_L \geq \sqrt{4RP}$. Applying duality rules (19) in (21), with $V_L = 0$:

$$\begin{aligned} \overline{T_C} &= RC \ln\left(\frac{\sqrt{V_H^2 + 4RP} + V_H}{2\sqrt{RP}}\right) \\ &\quad + \frac{CV_H\left(\sqrt{V_H^2 + 4RP} + V_H\right)}{4P} \end{aligned} \tag{22}$$

which after rearrangement reduces to T_C^{com}, given by (4). ■

2) LOADING TIME EXPRESSIONS

Following Theorem 1, CPL time equation for a supercapacitor model can be obtained from its corresponding RF charging time expression. It may be noted that CPL time expressions for simplified and 1-branch models respectively are valid only for $V_L \geq \max\left\{\sqrt{4R_S P}, \sqrt{\frac{R_P^2 P}{(R_P+R_S)}}\right\}$ and $V_L \geq \sqrt{R_{le}\frac{4P(R_1R_{le}+R_1^2)}{2(2R_1+R_{le})^2-R_1^2}}$. Interestingly, the loading time T_L^{ideal} for ideal model is, $T_L^{ideal}(V_H, V_L) = \frac{CV_L^2}{-2P} - \frac{CV_H^2}{-2P} = \frac{CV_H^2}{2P} - \frac{CV_L^2}{2P} = T_C^{ideal}(V_L, V_H)$.

Similar to temporal variation of voltage, relationship between loading current and CPL lime can be obtained using the duality rules. For example, using duality rules and $T_{C_I}^{simp}$ expression given by (10), time $T_{L_I}^{simp}$, during which the energy stored in a fully charged supercapacitor (simplified model) $V_C(t = 0) = V_H$ reduces to E_{min}, or loading current I increases from $I_L = \frac{V_H - \sqrt{V_H^2 - 4R_S P}}{2R_S}$ to $I(t = T_{L_I}^{simp}) = I_H$ is given as: $T_{L_I}^{simp} = T_{I_{load}}^{simp}(I_H) - T_{I_{load}}^{simp}(I_L)$, where $T_{I_{load}}^{simp}(I) = R_P C\left[\ln(I) - \frac{(R_P+2R_S)\ln(-P-I^2[R_S+R_P])}{2(R_P+R_S)}\right]$.

V. EXPERIMENTAL VALIDATION

Here we experimentally validate the assumptions in the analysis of renewable energy cycle.

A. RF CHARGING PROCESS AND PRACTICAL SUPERCAPACITOR MODEL PARAMETER ESTIMATION

RF charging as a constant-power charging process has been experimentally validated with commercial 50 mF supercapacitor in our recent work [18]. The circuit model parameters of the two supercapacitors 4.7 F and 50 F, given in Table 2 and used later in our simulations have been experimentally validated in [26] and [37], respectively.

TABLE 2. Circuit model parameters [26], [37].

Case	Parameter	Value	Case	Parameter	Value	Case	Parameter	Value	Case	Parameter	Value
Commercial model			Practical 1-branch model			Practical 3-branch model			Practical 3-branch model		
4.7 F	C	4.7 F	4.7 F	C_1	2.62 F	4.7 F	C_V	$0.945\frac{F}{V}$	50 F	C_V	$5.1\frac{F}{V}$
	R	0.178 Ω		C_V	$0.945\frac{F}{V}$		C_1	2.62 F		C_1	42.5 F
50 F	C	50 F		R_1	0.178 Ω		R_1	0.178 Ω		R_1	16 mΩ
	R	0.02 Ω		R_{le}	1030 Ω		C_2	1.45 F		C_2	10.5 F
Simplified model			50 F	C_1	42.5 F		R_2	94.2 Ω		R_2	112 Ω
4.7 F	C	4.06 F		C_V	$5.1\frac{F}{V}$		C_3	3.88 F		C_3	4 F
	R_S	0.8 Ω		R_1	16 mΩ		R_3	1030 Ω		R_3	628 Ω
	R_P	2010 Ω		R_{le}	36 kΩ		R_{le}	1030 Ω		R_{le}	36 kΩ

B. CONSTANT-POWER LOADING

We have undertaken systematic experiments to validate the CPL behavior of the field node, as assumed in Sections IV-B.

We have used Libelium Waspmote PRO V1.2 [38] and measured its consumption during the sensing state with toxic gas sensors *CO* and NO_2. The experimental setup (Fig. 6(a)) comprises of: i) wireless field node (Waspmote, Gas Sensors: MiCS-2710 (NO_2), TGS2442 (*CO*), communication module: Digi XBee Series 2, 2.4 GHz 5 dBi antenna, 2 GB microSD memory card); ii) DC voltage supply (Instek GPD-3303S); iii) multi-meter (HP34401A); iv) a low-value resistor (0.18Ω). DC supply, wireless node, and resistor are connected in series, while the multi-meter is connected in parallel to the resistor for measuring voltage. Low-value resistor is used to find the current consumed by the node without causing loading effect. The supply is varied from 3.3 V to 4.2 V (operational range).

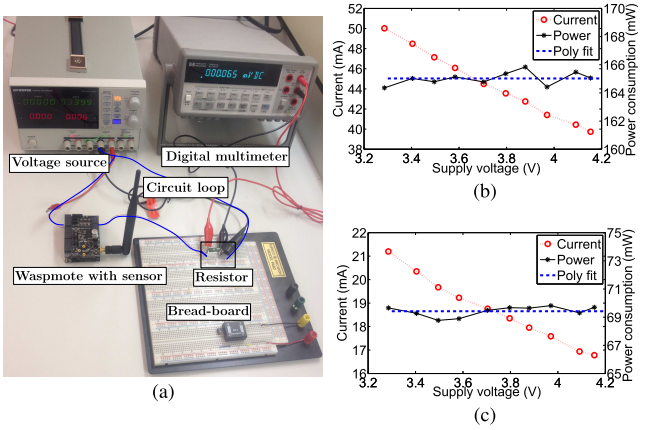

FIGURE 6. Experimental validation of constant-power loading process. (a) Experimental set up. (b) NO_2 gas sensor. (c) *CO* gas sensor.

The measured current consumption readings plotted in Figs. 6(b) and 6(c) for field node in *active* state include the consumption of processing module (≈ 15 mA), gases board, gas sensors, memory, but not the consumption of the communication module as it is disabled during sensing. Also, the current readings plotted are the average consumptions during the typical response duration of each sensor: 30 sec for NO_2 sensor and 1 sec for *CO* sensor [38]. The current readings are calculated by averaging the recorded $\left(\frac{V_{0.18}}{0.18}\right)$ readings for each supply voltage value. The plots also show that the current drawn by the Waspmote decreases with increasing supply voltage.

Power consumption of the Waspmote for each sensor during the *active* state is obtained by multiplying the supply voltage with the corresponding current consumption. The power consumption values are also plotted in Figs. 6(b) and 6(c) along with its zero-degree polynomial (constant function) fit. The normalized percentage change in the measured powers with respect to their mean (or poly-fit) values are respectively 0.21 and 0.41 for NO_2 and *CO* gases. The results show that, the power consumption during active state of the Waspmote for monitoring both the gases can be very closely approximated by a constant function, thereby validating the CPL behavior.

C. VALIDATION OF THE PROPOSED REC CIRCUIT MODEL

Here, to validate the proposed REC circuit model, we present the measurement results for charging and discharging of 40 F Lithium-ion capacitor LIC-1235R-3R8406 with

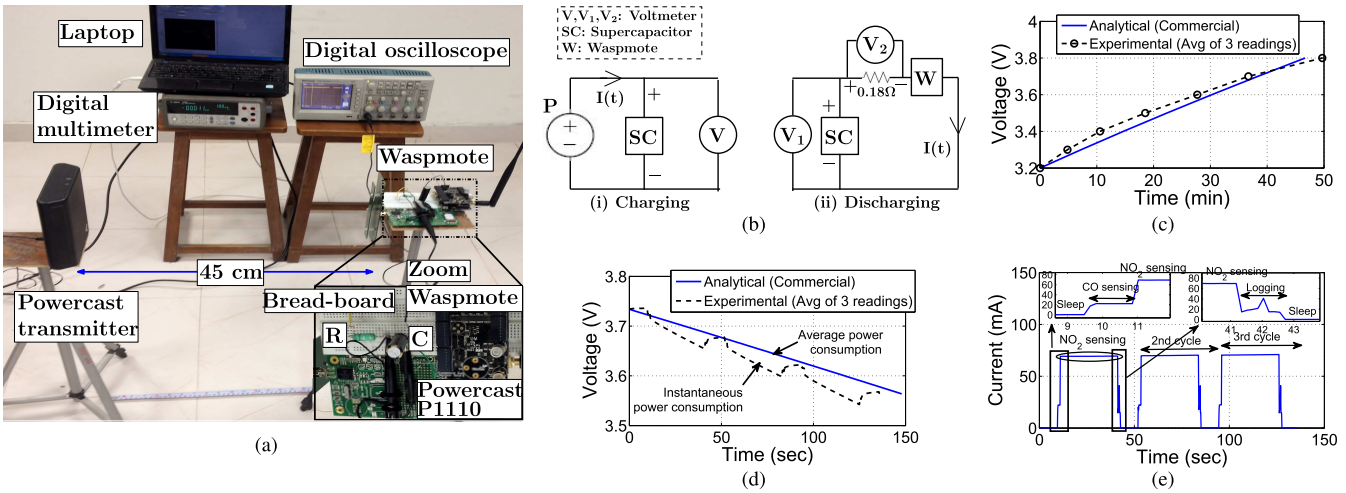

FIGURE 7. Experimental results for charging and discharging cycle in commercial supercapacitor model. (a) Experimental set up. (b) Measurement circuit. (c) Charging voltage variation. (d) Loading voltage variation. (e) Loading current variation.

ESR = 0.15 Ω (considering commercial supercapacitor model).

The experimental setup is shown in Fig. 7(a). It consists of three main components: (i) the RF source, which is a Powercast transmitter [34] placed 45 cm away from the end node and transmits with Effective Isotropic Radiated Power (EIRP) = 3 W at 915 MHz; (ii) the wireless field node, which includes Powercast P1110 RFEH circuit and 40 F supercapacitor, in addition to the basic components as indicated in Section V-B; (iii) the measurement circuit comprising of a digital oscilloscope (Tektronix TDS 2024B), multi-meter (Agilent 34405A), laptop (for recording measurements using NI LabVIEW), breadboard, and a low-value precision resistor (0.18 Ω). The measurement circuits for charging and discharging operations are shown in Fig. 7(b). For wireless charging of the node, the RF source transmits at 3 W, until the supercapacitor voltage reaches 3.8 V (maximum usable voltage). With path loss exponent taken as 2 (which is true for short transmitter-receiver distance), the received RF power is 41.03 mW. This yields an RF-to-DC rectification efficiency of 72.4% [34] and harvested DC power as $P = 29.70$ mW. The measured variation of capacitor voltage along with the analytical results obtained from Section IV-A.2 with $P = 29.70$ mW, $C = 40$ F, $R = 0.15$ Ω is plotted in Fig. 7(c). It is observed that the analytical results for commercial model closely match with experimental results – thereby validating the constant-power charging analysis. As noted in [26] and [27], more closer match of the analytical results with the measured values are expected for practical supercapacitor models that incorporate the nonidealities attributed to substantial leakage currents.

The capacitor voltage and loading current (individual state current consumption for Waspmote) results for discharging cycle are presented in Fig. 7(d) and 7(e), respectively. The measured results are obtained over three cycles, each comprising of a *sleep* state (10 sec), followed by *CO* and NO_2 *sensing* with respective response duration of 1 sec and 30 sec. The sensed readings are stored in the SD card during the *logging* state. Fig. 7(d) plots the variation of capacitor voltage with time. The experimental results are based on the instantaneous values, whereas the analytical results for commercial model are based on the average power consumption of the field node. The results show a close match between analytical and experimental readings – thereby validating CPL assumption. However, as discussed in Section IV and shown later in Section VI, practical models offer much better match by incorporating the nonidealities attributed to supercapacitor charging and discharging behaviors. These nonidealities include sudden rise and fall in supercapacitor voltage (see Fig. 7(d)) during state transitions (shown in Fig. 7(e)) due to the internal charge redistribution between different equivalent internal capacitors [26], [27].

In summary, through experimental validation of the proposed REC circuit model in this section, we have motivated the need for the analysis of practical supercapacitor models.

VI. SIMULATION MODEL FOR REC CHARACTERIZATION, ITS ANALYTICAL VERIFICATION, AND RESULTS

A. SIMULATION MODEL

As discussed in Section IV-A, to deal with the REC characterization of modern supercapacitor models that are analytically-intractable, we have developed a generic simulation framework. This proposed simulation model can provide RF charging and loading times for practical supercapacitor model with any level of complexity in design.

The simulation model provides voltage and current numerical values as a function of time, which can be stored in the iDEM memory for estimating the charging time T_C and revisit (loading) time T_L based on the values of V_H and V_L. Although there is no closed-form expressions of T_C and T_L available for highly complex but realistic models, this simulation model, which incurs one-time computation cost, provides

an accurate estimate of the charging time and node lifetime.

We have used the trapezoidal rule, which is based on the principle of approximating the region under the graph of the integrand as a trapezoid and then calculating its area. Voltage across supercapacitor $V_C(t)$ at time t can be approximated as:

$$\frac{1}{C}\int_{t_0}^{t} I(\tau)\,d\tau + V_C(t_0) \approx \frac{t-t_0}{2C}\left[I(t)+I(t_0)\right] + V_C(t_0)\,. \tag{23}$$

The simulation flow given in Fig. 8 involves 3 steps:

- *Initialization* of voltage across the capacitor(s) and resistor(s) at time $t = 0$ along with the branch current values.
- *Recursion*, which involves the usage of update equations for deriving voltage and current expressions for the nth time instant using the current and voltage expressions at $n-1$ and $n-2$ time instants. Here, $t_n - t_{n-1} = \Delta t \ll 1$ is the step size used in the simulation. The initialization and update equations for constant-power charging and CPL for various supercapacitor models are respectively given in Table 3 and Table 4. In the simulation model, $\Delta t = 0.05$ sec, $t_0 = 0$ sec, and initial update for $t = \Delta t$ is found by using the initial ($t = t_0$) current and voltage values. The equations mentioned in Tables 3 and 4 are obtained using the KVL equations given in Section IV, approximation (23), basic circuit laws, and by solving polynomial equation of second degree to find $I(t)$.
- *Termination*, when $t = T_C$ (respectively, $t = T_L$) while RF charging (respectively, loading).

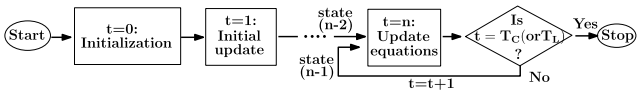

FIGURE 8. Simulation flow.

B. ANALYTICAL VERIFICATION AND SIMULATION RESULTS

The accuracy of the simulation model in estimating the charging time and loading time is validated for the supercapacitor models (ideal, commercial, simplified, and 1-branch) that have the closed-form analytical expressions. Figs. 9 and 10(a) show that the charging time T_C variation with $P = 0.12$ W obtained from the proposed simulation model closely matches the analytical equations developed in Section IV-A. Root mean square error (RMSE) of the analytical RF charging equations with respect to the results obtained from the simulation model for ideal, commercial, simplified, and 1-branch models are respectively 0.0797, 0.0727, 0.0691, and 0.0573, which are within the allowable upper limit of 0.08 for a model to be considered as good fit [39]. In the same figures, the proposed simulation model is also used for deriving loading and charging time for analytically-intractable 3-branch model. These values are utilized in estimating the sustainable network size for perpetual operation in the next section. Fig. 10(a) also plots the energy stored in various branches of 3-branch model,

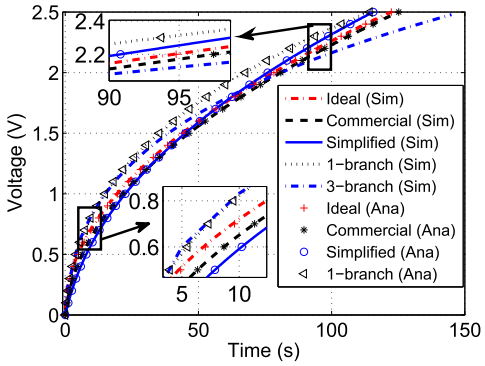

FIGURE 9. RF charging of 4.7 F supercapacitor (cf. Table 2).

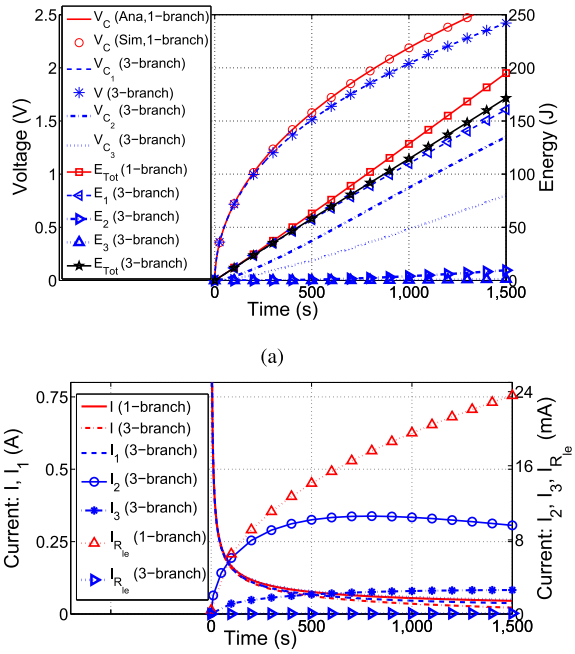

FIGURE 10. RF charging of 50 F supercapacitor (cf. Table 2). (a) Capacitor voltage variation. (b) Charging current variation.

which illustrates that most of the energy is stored in the first branch (C_1 and C_v), followed by the second branch.

Figs. 10(b) show the charging current $I(t)$ versus time. As shown in Fig. 10(b), the current across the second and third branches ($I_2(t)$ and $I_3(t)$) in 3-branch model along with $I_{R_{le}}(t)$ across the leakage resistor R_{le} in 1-branch and 3-branch models increase with time. However, for $t > 800$ sec, $I_2(t)$ decreases with time because the charge starts to get accumulated in the delayed branch also [26], [27].

Figs. 11(a) and 11(b) show the charging time T_C variation in different supercapacitor models with $V_L = 2$ V, $V_H = 2.5$ V, and P varied as 0.12 W, 0.055 W, and 0.025 W for different iDEM recharging distance: 45 cm, 66 cm, and 100 cm. The performance of simplified, practical 1-branch, and 3-branch models incorporate the long-term behavior very differently from the ideal and commercial models. For exam-

TABLE 3. Constant-power charging initialization and update equations.

Model	Initialization	Update Equations
Ideal	$I(t_0)=\sqrt{\frac{PC}{2t_0}},\quad V_C(t_0)=0$	$I(t)=\frac{P}{\frac{\Delta t}{2C}[I(t-1)+I(t-2)]+V_C(t-1)},\quad V_C(t)=\frac{\Delta t}{2C}[I(t-1)+I(t)]+V_C(t-1)$
Commercial	$I(t_0)=\sqrt{\frac{P}{R}},\quad V_C(t_0)=0$	$I(t)=\frac{P}{RI(t)+\frac{\Delta t}{2C}[I(t-1)+I(t)]+V_C(t-1)},\quad V_C(t)=\frac{\Delta t}{2C}(I(t-1)+I(t))+V_C(t-1)$
Simplified	$I(t_0)=\sqrt{\frac{P}{R_S}}$ $V_C(t_0)=0,\quad I_{R_P}(t_0)=0$	$I(t)=\frac{P}{R_S I(t)+\frac{\Delta t}{2C}\left[I(t-1)+I(t)-I_{R_P}(t-2)-I_{R_P}(t-1)\right]+V_C(t-1)},$ $V_C(t)=\frac{\Delta t}{2C}\left[I(t-1)+I(t)-I_{R_P}(t-2)-I_{R_P}(t-1)\right]+V_C(t-1),$ $V(t)=V_C(t)+R_S I(t),\quad I_{R_P}(t)=\frac{V_C(t)}{R_P}$
1- branch	$I(t_0)=\sqrt{\frac{P(R_1+R_{le})}{R_1R_{le}}}$ $V_C(t_0)=0,\quad I_{R_{le}}(t_0)=I(t_0)\frac{R_1}{R_1+R_{le}}$	$I(t)=P\Big[R_1(I(t)-I_{R_{le}}(t-1))+\frac{\Delta t\left[I(t-1)+I(t)-I_{R_{le}}(t-1)-I_{R_{le}}(t-2)\right]}{2[C_1+C_vV_C(t-1)]}$ $+V_C(t-1)\Big]^{-1},\quad V_{R_{le}}(t)=R_{le}I_{R_{le}}(t),\quad I_{R_{le}}(t)=\frac{P}{R_{le}I(t)},$ $V_C(t)=\frac{\Delta t\left[\sum_{j=0}^{1}\left(I(t-j)-I_{R_{le}}(t-j)\right)\right]}{2[C_1+C_vV_C(t-1)]}+V_C(t-1),$ $V(t)=V_C(t)+R_1\left[I(t)-I_{R_{le}}(t)\right]$
3- branch	$I(t_0)=\sqrt{P\left(\frac{S_R}{R_1R_2R_3R_{le}}\right)}$ where $S_R=R_1(R_2(R_3+R_{le})+$ $R_3R_{le})+R_2R_3R_{le}$ $V_{C_1}(t_0)=0,\quad V_{C2}(t_0)=0,\quad V_{C3}(t_0)=0$ $I_2(t_0)=I(t_0)\frac{R_1R_3R_{le}}{S_R}$ $I_3(t_0)=I(t_0)\frac{R_1R_2R_{le}}{S_R},\quad I_{R_{le}}(t_0)=I(t_0)\frac{R_1R_2R_3}{S_R}$	$I(t)=P\Big[R_1(I(t)-I_2(t-1)-I_3(t-1)-I_{R_{le}}(t-1))+\frac{\Delta t}{2(C_1+C_vV_{C_1}(t-1))}$ $\Big\{I(t-1)+I(t)-I_2(t-1)-I_3(t-1)-I_{R_{le}}(t-1)-I_2(t-2)-I_3(t-2)$ $-I_{R_{le}}(t-2)\Big\}+V_{C_1}(t-1)\Big]^{-1},$ $V_{Cj}(t)=\frac{\Delta t[V(t-1)]+R_jC_2V_{Cj(t-1)}}{R_jC_j+\Delta t},\forall j\in(2,3),$ $I_{R_{le}}(t)=\frac{P}{R_{le}I(t)},\quad V_{R_{le}}(t)=R_{le}I_{R_{le}}(t),\quad I_j(t)=\frac{V(t-1)-V_{Cj}(t)}{R_j},\forall j\in(2,3)$ $V_{C_1}(t)=\frac{\Delta t\left[\sum_{j=0}^{1}\left(I(t-j)-I_2(t-j)-I_3(t-j)-I_{R_{le}}(t-j)\right)\right]}{2(C_1+C_vV_{C_1}(t-1))}+V_{C_1}(t-1),$ $V(t)=V_{C_1}(t)+R_1\left[I(t)-I_2(t)-I_3(t)-I_{R_{le}}(t)\right]$

TABLE 4. Constant-power loading initialization and update equations.

Model	Initialization	Update Equations
Ideal	$V_C(t_0)=2.5,\quad I(t_0)=0$	$I(t)=-\frac{P}{\frac{\Delta t}{2C}[I(t-1)+I(t-2)]+V_C(t-1)},\quad V_C(t)=-\frac{\Delta t}{2C}[I(t-1)+I(t)]+V_C(t-1)$
Commercial	$V_C(t_0)=2.5$ $I(t_0)=\frac{V_C(t_0)-\sqrt{V_C^2(t_0)-4RP}}{2R}$	$I(t)=\frac{P}{-RI(t)-\frac{\Delta t}{2C}[I(t-1)+I(t)]+V_C(t-1))},\quad V_C(t)=-\frac{\Delta t}{2C}[I(t-1)+I(t)]+V_C(t-1))$
Simplified	$V_C(t_0)=2.5,\quad I_{R_P}(t_0)=\frac{V_C(t_0)}{R_P}$ $I(t_0)=\frac{V_C(t_0)-\sqrt{V_C^2(t_0)-4R_SP}}{2R_S}$	$I(t)=\frac{P}{-R_sI(t-1)-\left(\frac{\Delta t}{2C}\left[I(t-2)+I(t-1)+I_{R_P}(t-2)+I_{R_P}(t-1)\right]\right)+V_C(t-1)},$ $V_C(t)=-\frac{\Delta t}{2C}\left[I(t-1)+I(t)+I_{R_P}(t-1)+I_{R_P}(t-2)\right]+V_C(t-1),\quad I_{R_P}(t)=\frac{V_C(t)}{R_p},$ $V(t)=V_C(t)-R_sI(t)$
1- branch	$V_C(t_0)=2.5$ $I(t_0)=\frac{V_C(t_0)-\sqrt{V_C^2(t_0)-4R_1P}}{2R_1}$ $I_{R_{le}}(t_0)=0$	$I(t)=P\left[-\left[I(t)+I_{R_{le}}(t-1)\right]R_1-\frac{\Delta t\left[I(t-1)+I(t)+I_{R_{le}}(t-1)+I_{R_{le}}(t-2)\right]}{2[C1+CvV_C(t-1)]}+V_C(t-1)\right]^{-1}$ $I_{R_{le}}(t)=\frac{P}{R_{le}I(t)},\quad V_{R_{le}}(t)=R_{le}I_{R_{le}}(t),\quad V_C(t)=\Bigg[-\left[\frac{\Delta t\left[\sum_{j=0}^{1}\left(I(t-j)+I_{R_{le}}(t-j)\right)\right]}{2[C_1+C_vV_C(t-1)]}\right]$ $+V_C(t-1)\Bigg],\quad V(t)=V_C(t)-R_1(I(t)+I_{R_{le}}(t))$
3- branch	$V_{C_1}(t_0)=2.5$ $I(t_0)=\frac{V_{C_1}(t_0)-\sqrt{{V_{C_1}}^2(t_0)-4R_1P\left(1+\frac{R_1}{R_{le}}\right)}}{2R_1}$ $V(t_0)=V_{C_1}(t_0)-R_1\left[I(t_0)+\frac{V_{C_1}(t_0)}{R_{le}}\right]$ $V_{C_2}(t_0)=V(t_0),\qquad V_{C_3}(t_0)=V(t_0)$ $I_2(t_0)=0,\quad I_3(t_0)=0,\quad I_{R_{le}}(t_0)=\frac{V(t_0)}{R_{le}}$	$I(t)=P\Big[-R_1\left(I(t)+I_2(t-1)+I_3(t-1)+I_{R_{le}}(t-1)\right)-\frac{\Delta t}{2(C_1+C_vV_{C_1}(t-1))}[I(t-1)$ $+I(t)+I_2(t-1)+I_2(t-2)+I_3(t-1)+I_3(t-2)+I_{R_{le}}(t-1)+I_{R_{le}}(t-2)]$ $+V_{C_1}(t-1)\Big]^{-1},\quad I_{R_{le}}(t)=\frac{P}{R_{le}I(t)},\qquad V_{R_{le}}(t)=R_{le}I_{R_{le}}(t)$ $V_{Cj}(t)=\frac{\Delta t[V(t-1)]+R_jC_2V_{Cj(t-1)}}{R_jC_j+\Delta t},\forall j\in(2,3),\qquad I_j(t)=\frac{V_{Cj}(t)-V(t-1)}{R_j},\forall j\in(2,3)$ $V_{C_1}(t)=\frac{-\Delta t\left[\sum_{i=0}^{1}\left(I(t-j)+I_2(t-j)+I_3(t-j)+I_{R_{le}}(t-j)\right)\right]}{2(C_1+C_vV_{C_1}(t-1))}+V_{C_1}(t-1),$ $V(t)=V_{C_1}(t)-R_1(I(t)+I_2(t)+I_3(t)+I_{R_{le}}(t))$

ple, T_C for ideal model is respectively 50.47% and 30.47% lesser than the practical 3-branch model in 4.7 F and 50 F supercapacitors.

Figs. 12(a) and 12(b) plot the variation of capacitor voltage and loading current I with time for $P = 0.12$ W. The results from the developed simulation model closely match with that analytically obtained using duality principle (Section IV-B). RMSE of 0.0358, 0.0177, 0.0183, and 0.0268, respectively in T_L values obtained from analytical equations and simulation model for ideal, commercial, simplified, and 1-branch

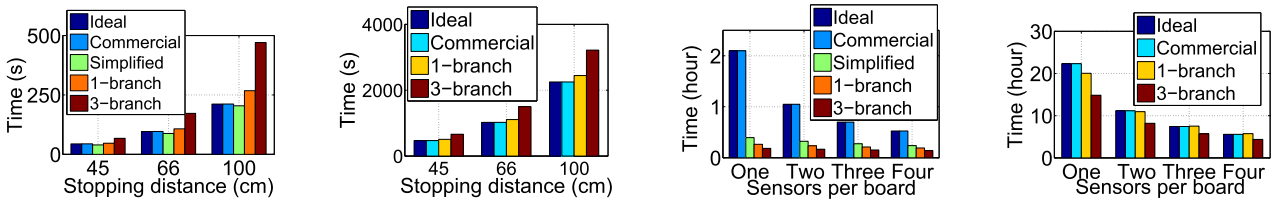

FIGURE 11. RF charging and constant-power loading time comparison. (a) T_C for 4.7 F. (b) T_C for 50 F. (c) T_L for 4.7 F. (b) T_L for 50 F.

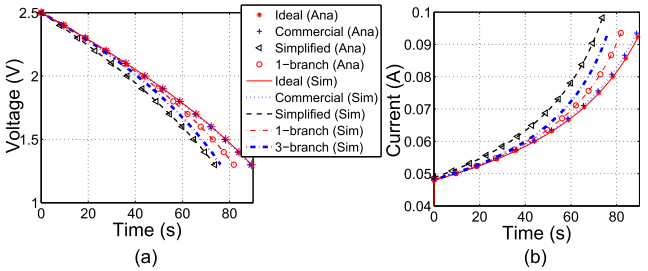

FIGURE 12. Constant-power loading of 4.7F supercapacitor (cf. Table 2). (a) Capacitor voltage variation. (b) Current variation.

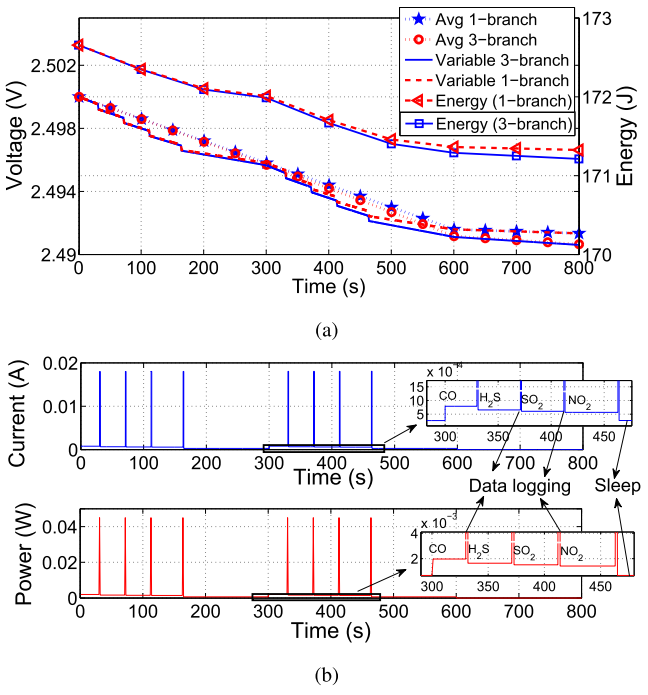

FIGURE 13. Constant-power loading of 50 F supercapacitor (cf. Table 2). (a) Capacitor voltage variation. (b) Current and power variation.

models, validate that the proposed simulation model is a good fit [39] with the analytical expressions derived for both T_L and T_C.

Next we show the impact of state-dependent energy consumption of a field node. Figs. 13(a) shows the temporal variation capacitor voltage ($V_C(t)$ or $V_{C_1}(t)$) with 50 F supercapacitor for 1-branch and 3-branch models along

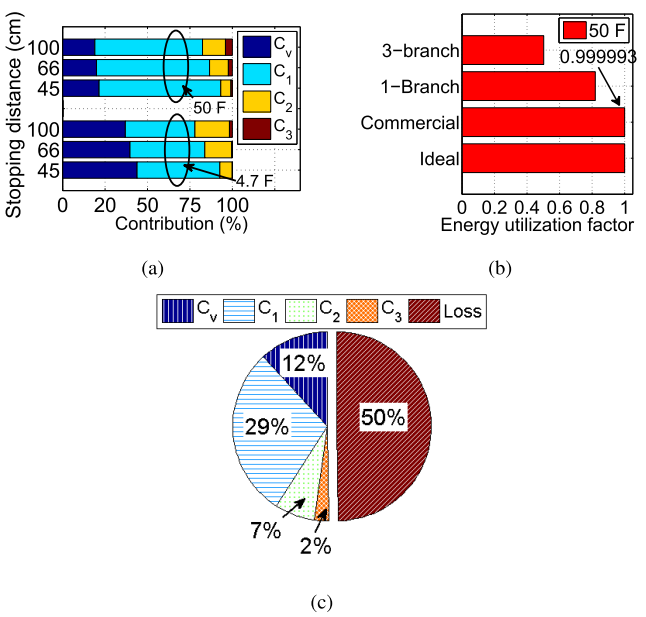

FIGURE 14. Simulation results for energy distribution. (a) Component contribution. (b) Utilization factor. (c) Distribution for 50 F.

with the energy stored $\left(E_{s_1}^{pr_{1b}} = \frac{1}{2}\left(C_1 + C_v V_C\right) V_C^2\right.$ and $\left.E_{s_1}^{pr_{3b}} = \frac{1}{2}\left(C_1 + C_v V_{C_1}\right) V_{C_1}^2\right)$ in the first branch for both instantaneous and average power consumption scenarios. After $t = 600$ sec, the load is removed from the circuit to show the leakage and self-discharge effects (cf. Fig. 13(a)). The temporal variation of loading current $I(t)$ (for 1-branch model) and power P for each sensor are shown in Fig. 13(b). As shown in Fig. 13(a) the state-dependent average and instantaneous (or variable) power consumptions has approximately the same nature after $t = 600$ sec, which implies that $P = P_{cons}^{avg}$ can be considered during CPL-based node lifetime estimation.

Figs. 11(c) and 11(d) show the loading time T_L variation for different supercapacitor models with $V_L = 2$ V, $V_H = 2.5$ V, and $P = 0.7n$ mW, where n is the number of sensors per node (calculated using the consumption model given in Section III-B.2). The results show that, T_L for 3-branch model are respectively 85.24% and 28.80% lesser than the T_L obtained using the ideal model with 4.7 F and 50 F supercapacitors – which are very significant differences.

Effective energy utilization is one of the major factors affecting the performance of energy harvesting nodes. In Fig. 14(a), the distribution of energy among different capacitors in the 3-branch model with varying d_{stop} values shows that most of the energy is stored in the first branch. The utilization factor $UF = \frac{E_{stored}}{E_{stored}+E_{lost}}$ along with E_{stored} for different models in Fig. 14(b) show that, UF with ideal and commercial models are almost 1, whereas for 3-branch model it is less than 0.5. Fig. 14(c) presents the distribution of total supplied energy E_{supp} in 3-branch model, which indicates that the practical supercapacitors suffer from significant energy loss (about 50%) due to leakage. This can have a significant impact on perpetual network operation, as explained next.

VII. ESTIMATION OF SUSTAINABLE NETWORK SIZE

We now use the results on charging and discharging characteristics to find the RFEH-assisted pollution monitoring network size that can be supported by a single iDEM for uninterrupted operation. Network size is defined as follows:

Definition 6: Network size is defined as the number of field nodes that can be served in a manner that none of the nodes ever runs out of energy or buffer space.

Here, energy depletion is more critical because a node becomes nonfunctional if its energy level goes below E_{min}.

Based on the consumption in different operational states of a field node (Section III-B.2) and the expressions of T_C and T_L (Section VI), we obtain the lifetime of each node in the network. Using the node lifetime along with T_C and inter-node travel time, the network size is estimated. Below, we discuss the network model parameters for the network size estimation.

A. NETWORK MODEL

Field nodes are deployed over a square 5 km $\times$ 5 km field of area following the Poisson point process (PPP). We have considered PPP for sensor node deployment because it is the most widely used mathematical model for analyzing the performance of wireless adhoc and sensor networks with random topologies [40]. The speed of iDEM is taken 5 m/s. The charging time parameters taken from the experimental observations are: RF transmit power 3 W; operating frequency 915 MHz; transmitter and receiver antenna gains 6.1 dBi; supercapacitor value $C = 50$ F; $V_L = 2$ V and $V_H = 2.5$ V. The different cases considered are:

1) Sensing-Dependent Energy Consumption of the Field Nodes: Due to sensing-dependent variable energy consumption, some field nodes may require more frequent replenishment than the others, and as a result the iDEM needs to visit such nodes more frequently. To implement this randomness of the field nodes' energy consumption, we have considered three example cases:

Case A: All nodes consume nearly the same energy and have the same estimated revisit time; Case B: Some randomness in energy consumption is present in the network, due to which some nodes' consumption rate is about twice as compared to the others; and Case C: Due to additional degree of randomness, the nodes are divided in 3 groups. The number of visits in a tour of iDEM are: one for *group 1* nodes, two for *group 2*, and four for *group 3*. The three group sizes are equal in size and uniformly random distributed in space.

2) Stopping Distance d_{stop} of iDEM From the Node to be Charged: Due to small RFET range, the three stopping distances considered are: 45 cm, 66 cm and, 100 cm. This parameter determines T_C, because the values of harvested DC power P, calculated by considering Powercast $P1110$ RF-to-DC rectification efficiency [34] and path loss, for the three d_{stop} values are 0.12 W, 0.055 W, and 0.025 W, respectively.

3) Number of Sensors Per Node: (i) One sensor: CO having $P = P_{cons}^{avg} \approx 0.7$ mW; (ii) Two sensors: CO and NO_2 having $P = P_{cons}^{avg} \approx 1.4$ mW; (iii) Three sensors: CO, NO_2, and H_2S having $P = P_{cons}^{avg} \approx 2.1$ mW; (iv) Four sensors: CO, NO_2, H_2S, and SO_2 having $P = P_{cons}^{avg} \approx 2.8$ mW. This parameter influences the CPL time T_L.

4) Supercapacitor Models: Different models considered are: ideal, commercial, practical 1-branch and 3-branch models. Simplified model is not considered due to the unavailability of the corresponding circuit parameters for 50 F supercapacitor.

In order to serve the maximum number of nodes, iDEM should spend minimum time in traveling, i.e., the overall tour length should be minimized. In differential energy consumption scenarios, since conventional Traveling Salesman Problem (TSP)-based solutions cannot be used directly, three example TSP tours are considered: a) TSP tour 1 having only *group 3* field nodes; b) TSP tour 2 having *group 2* and *3* nodes; c) TSP tour 3 having nodes from all 3 groups. So, one complete schedule of iDEM will start TSP tour 1, followed by TSP tour 2, TSP tour 1, and finally TSP tour 3, so that *group 1, 2, and 3* nodes are served respectively once, twice, and four times in a single iDEM tour. The TSP tours are found using Genetic Algorithm. This iDEM schedule is then repeated, thus providing an uninterrupted network operation. Numerical results presented below are based on an average over 30 runs.

B. NUMERICAL RESULTS

Sustainable network size for different supercapacitor models under different degree of randomness in energy consumption are shown in Figs. 15, 16, and 17. The effect of recharging distance d_{stop} on network size is shown in the respective subfigures (a), (b), and (c). The results show that the network size with practical supercapacitor models is very different from the ideal or commercial models. Using commercial, 1-branch, and 3-branch models, the average number of nodes served with different number of sensors per node, d_{stop} values, and energy consumption cases are respectively 1.52% 14.18%, and 52.20% less than what can be supported using the ideal model.

The impact of energy consumption diversity on the sustainable network size can be realized from the fact that, in

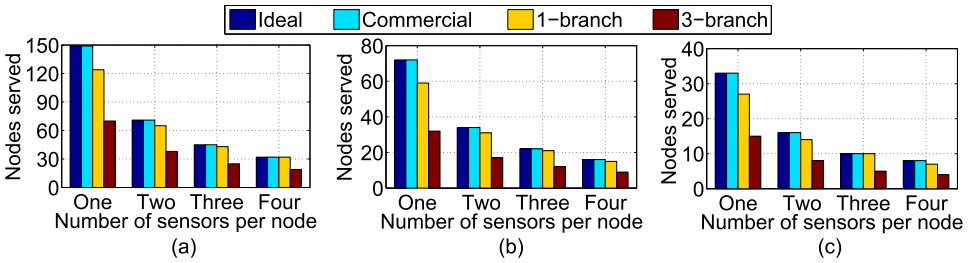

FIGURE 15. Case A: Only *group 1* nodes. (a) $d_{stop} = 45$ cm. (b) $d_{stop} = 66$ cm. (c) $d_{stop} = 100$ cm.

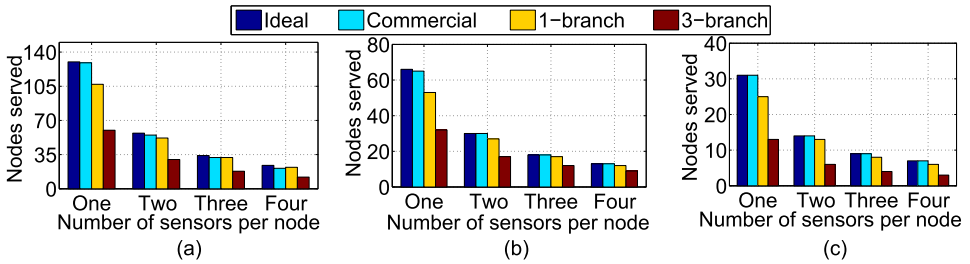

FIGURE 16. Case B: Both *group 1* and *group 2* nodes. (a) $d_{stop} = 45$ cm. (b) $d_{stop} = 66$ cm. (c) $d_{stop} = 100$ cm.

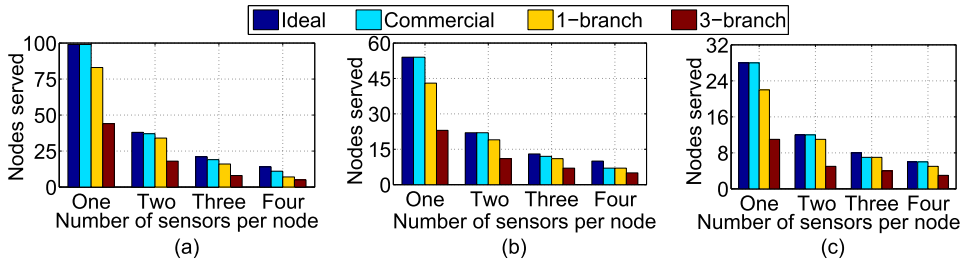

FIGURE 17. Case C: All three *group* of nodes considered. (a) $d_{stop} = 45$ cm. (b) $d_{stop} = 66$ cm. (c) $d_{stop} = 100$ cm.

cases B and C (Figs. 16 and 17) the network size supported by a single iDEM are respectively 16% and 40% lesser than in case A (Fig. 15). The harvested DC power P for recharging a field node sharply reduces with the increased iDEM recharging distance d_{stop}, causing an increased RF charging time and hence reduced sustainable network size. The average network size with d_{stop} as 66 cm and 100 cm are respectively 48.61% and 75.33% lesser than that with $d_{stop} = 45$ cm. Further, the number of sensors per node also has a great impact on the network size. In networks with two, three, and four sensors per node, the network size is 54.01%, 72.14%, and 80.74% less as compared to the networks with single sensor per node.

Table 5 shows that the average charging time T_C is comparable to the average traveling time for case C. In cases A and B with larger network size and lower degree of randomness in energy consumption, T_C is much higher than the traveling time, which is because, with increasing network size, the total charging time increases. The respective shares of T_C in a single iDEM tour schedule for cases A, B, and C are 86.98%, 73.90%, and 54.64%. The results show that, T_C is a major cost (more than 50%) that needs to be tackled in RFET-based energy replenishment techniques, as it plays a significant role in estimating the network size that can be supported by a single iDEM. Commercial and ideal supercapacitors have similar performances in terms of T_C and sustainable network size. However the performance of 1-branch and 3-branch models is very different. Also, the effect of leakage

TABLE 5. iDEM scheduling numerical results.

Case		Average T_C per node (hrs)	Average total T_C (hrs)	Average total travel time (hrs)	Average periodic schedule duration (hrs)	Average network size
Ideal	A	0.3464	9.9893	1.4670	11.6258	41.9250
	B		8.6123	2.9157		35.5222
	C		6.7028	4.8702		26.5528
Commercial	A	0.3465	9.9898	1.4670	11.6257	41.9194
	B		8.5847	3.0024		34.9083
	C		6.3021	4.9526		25.5917
1- branch	A	0.3760	9.4230	1.3996	11.0638	36.9667
	B		8.0272	2.9080		30.6556
	C		5.9828	5.0455		21.6306
3- branch	A	0.4983	6.9517	1.0877	8.2774	20.7917
	B		5.9211	2.1467		17.4722
	C		4.1072	4.0432		11.4528

and self-discharge leading to 50% energy loss is captured in T_L expression for practical supercapacitor models. The above results signify the importance of accurately estimating the circuit parameters and using the proposed RF charging and node lifetime formulations based on these practical supercapacitor models.

VIII. CONCLUDING REMARKS

In this work we have shown that the nonidealities in practical supercapacitors have significant impact on the performance of energy harvesting networks. To gain analytical insights on practical rechargeability constraints, REC circuit model has been proposed and RF charging time and node lifetime expressions for the practical supercapacitor models have been derived. The analytical circuit model for the REC has been validated through hardware experiments. Based on a duality principle, constant-power loading time has been derived from the RF charging time characteristics of the practical supercapacitors. To deal with more practical but analytically intractable supercapacitor models, a generic simulation model has been developed. The models developed for charging and loading time have been used to find the sustainable network size for green perpetual network operation of an energy-hungry sensor network, such as, pollution monitoring network. With the help of analytical and numerical results presented in this paper, we show that the lifetime of a typical RFEH-assisted pollution monitoring network with current consumption model given in Table 1 gets reduced by 28.80% on accounting the nonidealities, such as, self-discharge, leakage, and aging effects in practical supercapacitors. Further, the impact of leakage and aging effects of the practical supercapacitors for commercial wireless pollution monitoring field nodes with Mica2 mote, RF energy harvester, and antennas from Powercast demonstrate significant difference in terms of sustainable network size (e.g., 52% lesser network size with 3-branch model as compared to the ideal model) supported by a single iDEM.

The developed models and observations presented here will be useful in accurately planning and estimating the performance of green energy harvesting sensor networks.

APPENDIX A
CHARGING CURRENT VARIATION FOR 1-BRANCH MODEL

Applying KVL in Fig. 4(d) and using $V_C(t=0)=0$, gives:

$$\left[I_{R_{le}}(t)R_{le} - I_1(t)R_1\right]\cdot\left[C_1 + C_v\cdot V_C(t)\right] = \int_0^t I_1(t)dt \tag{A.1}$$

Using $V_C(t) = \frac{P}{I(t)} - I_1(t)R_1$, $I_{R_{le}}(t) = \frac{P}{I(t)R_{le}}$, $I_1(t) = I(t) - \frac{P}{I(t)R_{le}}$, and differentiating (A.1) with respect to t, we obtain:

$$(C_1+2Y_3)\frac{dI(t)}{dt}\left[R_1+\frac{PR_1}{[I(t)]^2R_{le}}+\frac{P}{I(t)^2}\right] = \frac{P}{I(t)R_{le}} - I(t) \tag{A.2}$$

where $Y_3 = C_v\left(\frac{P}{I(t)} - R_1\left[I(t) - \frac{P}{I(t)R_{le}}\right]\right)$. Solving (A.2), the time $T_{C_I}^{pr_{1b}}$ during which $I(t)$ falls from $I(t=0) = \sqrt{\frac{P(R_1\cdot R_{le})}{R_1+R_{le}}}$ to $I\left(T_{C_I}^{pr_{1b}}\right) = I_L$ is:

$$\begin{aligned}T_{C_I}^{pr_{1b}} &= \frac{1}{2R_{le}}\Bigg[R_{le}C_1\Bigg((2R_1+R_{le})\ln\left[\frac{PR_{le}}{R_1\left(\left[I_L\right]^2R_{le}-P\right)}\right] \\ &\quad + (R_1+R_{le})\ln\left[\frac{I_L^2}{Y_4}\right]\Bigg) - 4C_v\Bigg(\left[\tanh^{-1}\left(\frac{\sqrt{R_{le}}I_L}{\sqrt{P}}\right)\right. \\ &\quad \left.- \tanh^{-1}\left(\sqrt{\frac{R_{le}Y_4}{P}}\right)\right]\sqrt{PR_{le}^3}(2R_1+R_{le}) \\ &\quad + \frac{P(R_1+R_{le})^2}{I_L} + R_1R_{le}\left\{R_{le}\sqrt{Y_4}+I_LR_1\right\}\Bigg)\Bigg]\end{aligned} \tag{A.3}$$

where $Y_4 = \frac{P(R_1+R_{le})}{R_1R_{le}}$. It may be noted that, $T_{C_I}^{pr_{1b}}$ is a function of the current I_L. Following the similar approach current variation with time for CPL can also be obtained.

REFERENCES

[1] I. F. Akyildiz, W. Su, Y. Sankarasubramaniam, and E. Cayirci, "Wireless sensor networks: A survey," *Comput. Netw.*, vol. 38, no. 4, pp. 393–422, Mar. 2002.
[2] W. Zhao *et al.*, "An energy harvesting system surveyed for a variety of unattended electronic applications," *Solid-State Electron.*, vol. 79, pp. 233–237, Jan. 2013.
[3] S. Basagni, M. Y. Naderi, C. Petrioli, and D. Spenza, "Wireless sensor networks with energy harvesting," in *Mobile Ad Hoc Networking: Cutting Edge Directions*, S. Basagni, M. Conti, S. Giordano, and I. Stojmenovic, Eds. Hoboken, NJ, USA: Wiley, Mar. 2013, ch. 20, pp. 703–736.
[4] X.-Y. Liu *et al.*, "CDC: Compressive data collection for wireless sensor networks," *IEEE Trans. Parallel Distrib. Syst.*, vol. 26, no. 8, pp. 2188–2197, Aug. 2015.
[5] L. He, Z. Yang, J. Pan, L. Cai, J. Xu, and Y. Gu, "Evaluating service disciplines for on-demand mobile data collection in sensor networks," *IEEE Trans. Mobile Comput.*, vol. 13, no. 4, pp. 797–810, Apr. 2014.
[6] S. De and R. Singhal, "Toward uninterrupted operation of wireless sensor networks," *Computer*, vol. 45, no. 9, pp. 24–30, Sep. 2012.
[7] A. A. Eteng, S. K. A. Rahim, and C. Y. Leow, "Wireless nonradiative energy transfer: Antenna performance enhancement techniques," *IEEE Antennas Propag. Mag.*, vol. 57, no. 3, pp. 16–22, Jun. 2015.
[8] L. Xie, Y. Shi, Y. T. Hou, and H. D. Sherali, "Making sensor networks immortal: An energy-renewal approach with wireless power transfer," *IEEE/ACM Trans. Netw*, vol. 20, no. 6, pp. 1748–1761, Dec. 2012.
[9] S. He, J. Chen, F. Jiang, D. K. Y. Yau, G. Xing, and Y. Sun, "Energy provisioning in wireless rechargeable sensor networks," *IEEE Trans. Mobile Comput.*, vol. 12, no. 10, pp. 1931–1942, Oct. 2013.
[10] T. Paing *et al.*, "Wirelessly-powered wireless sensor platform," in *Proc. Eur. Microw. Conf.*, Munich, Germany, Oct. 2007, pp. 999–1002.
[11] B. Gurakan, O. Ozel, and S. Ulukus, "Optimal energy and data routing in networks with energy cooperation," *IEEE Trans. Wireless Commun.*, vol. 15, no. 2, pp. 857–870, Feb. 2016.
[12] X. Lu, P. Wang, D. Niyato, D. I. Kim, and Z. Han, "Wireless networks with RF energy harvesting: A contemporary survey," *IEEE Commun. Surveys Tuts.*, vol. 17, no. 2, pp. 757–789, May 2015.
[13] P.-H. Hsieh, C.-H. Chou, and T. Chiang, "An RF energy harvester with 44.1% PCE at input available power of −12 dBm," *IEEE Trans. Circuits Syst. I, Reg. Papers*, vol. 62, no. 6, pp. 1528–1537, Jun. 2015.
[14] X. Huang and N. Ansari, "Energy sharing within EH-enabled wireless communication networks," *IEEE Wireless Commun.*, vol. 22, no. 3, pp. 144–149, Jun. 2015.
[15] D. Mishra and S. De, "Optimal relay placement in two-hop RF energy transfer," *IEEE Trans. Commun.*, vol. 63, no. 5, pp. 1635–1647, May 2015.
[16] X. Chen, Z. Zhang, H.-H. Chen, and H. Zhang, "Enhancing wireless information and power transfer by exploiting multi-antenna techniques," *IEEE Commun. Mag.*, vol. 53, no. 4, pp. 133–141, Apr. 2015.

[17] D. Mishra, S. De, S. Jana, S. Basagni, K. Chowdhury, and W. Heinzelman, "Smart RF energy harvesting communications: Challenges and opportunities," *IEEE Commun. Mag.*, vol. 53, no. 4, pp. 70–78, Apr. 2015.
[18] D. Mishra, S. De, and K. R. Chowdhury, "Charging time characterization for wireless RF energy transfer," *IEEE Trans. Circuits Syst. II, Exp. Briefs*, vol. 62, no. 4, pp. 362–366, Apr. 2015.
[19] J. Polastre, J. Hill, and D. Culler, "Versatile low power media access for wireless sensor networks," in *Proc. Int. Conf. Embedded Netw. Sensor Syst.*, 2004, pp. 95–107.
[20] P. Gupta, K. Kandakatla, S. De, and S. Jana, "Feasibility analysis on integrated recharging and data collection in pollution sensor networks," in *Proc. Nat. Conf. Commun. (NCC)*, New Delhi, India, Feb. 2013, pp. 1–5.
[21] V. Shnayder, M. Hempstead, B. Chen, G. W. Allen, and M. Welsh, "Simulating the power consumption of large-scale sensor network applications," in *Proc. ACM SenSys*, New York, NY, USA, Nov. 2004, pp. 188–200.
[22] C. Renner, J. Jessen, and V. Turau, "Lifetime prediction for supercapacitor-powered wireless sensor nodes," in *Proc. 8th GI/ITG KuVS Fachgespräch Drahtlose Sensornetze (FGSN)*, Hamburg, Germany, Aug. 2009, pp. 55–58.
[23] X. Jiang, J. Polastre, and D. Culler, "Perpetual environmentally powered sensor networks," in *Proc. 4th Int. Symp. Inf. Process. Sensor Netw.*, Los Angeles, CA, USA, Apr. 2005, pp. 463–468.
[24] J. M. Miller, "Electrical and thermal performance of the carbon-carbon ultracapacitor under constant power conditions," in *Proc. IEEE Veh. Power Propul. Conf.*, Arlington, TX, USA, Sep. 2007, pp. 559–566.
[25] R. L. Spyker and R. M. Nelms, "Analysis of double-layer capacitors supplying constant power loads," *IEEE Trans. Aerosp. Electron. Syst.*, vol. 36, no. 4, pp. 1439–1443, Oct. 2000.
[26] A. S. Weddell, G. V. Merrett, T. J. Kazmierski, and B. M. Al-Hashimi, "Accurate supercapacitor modeling for energy harvesting wireless sensor nodes," *IEEE Trans. Circuits Syst. II, Exp. Briefs*, vol. 58, no. 12, pp. 911–915, Dec. 2011.
[27] L. Zubieta and R. Bonert, "Characterization of double-layer capacitors for power electronics applications," *IEEE Trans. Ind. Appl.*, vol. 36, no. 1, pp. 199–205, Jan. 2000.
[28] V. Musolino, L. Piegari, and E. Tironi, "New full-frequency-range supercapacitor model with easy identification procedure," *IEEE Trans. Ind. Electron.*, vol. 60, no. 1, pp. 112–120, Jan. 2013.
[29] D. Torregrossa, M. Bahramipanah, E. Namor, R. Cherkaoui, and M. Paolone, "Improvement of dynamic modeling of supercapacitor by residual charge effects estimation," *IEEE Trans. Ind. Electron.*, vol. 61, no. 3, pp. 1345–1354, Mar. 2014.
[30] L. Xie *et al.*, "A mobile platform for wireless charging and data collection in sensor networks," *IEEE J. Sel. Areas Commun.*, vol. 33, no. 8, pp. 1521–1533, Aug. 2015.
[31] M. Zhao, J. Li, and Y. Yang, "A framework of joint mobile energy replenishment and data gathering in wireless rechargeable sensor networks," *IEEE Trans. Mobile Comput.*, vol. 13, no. 12, pp. 2689–2705, Dec. 2014.
[32] S. Guo, C. Wang, and Y. Yang, "Joint mobile data gathering and energy provisioning in wireless rechargeable sensor networks," *IEEE Trans. Mobile Comput.*, vol. 13, no. 12, pp. 2836–2852, Dec. 2014.
[33] L. Fu, L. He, P. Cheng, Y. Gu, J. Pan, and J. Chen, "ESync: Energy synchronized mobile charging in rechargeable wireless sensor networks," *IEEE Trans. Veh. Technol.*, accessed Sep. 2015, DOI: 10.1109/TVT.2015.2481920
[34] Powercast Corporation. [Online]. Available: http://www.powercastco.com, accessed Aug. 10, 2015.
[35] L. Chen *et al.*, "Range extension of passive wake-up radio systems through energy harvesting," in *Proc. IEEE ICC*, Budapest, Hungary, Jun. 2013, pp. 1549–1554.
[36] *MAX1674/MAX1675/MAX1676 Full Data Sheet*. [Online]. Available: http://datasheets.maximintegrated.com/en/ds/MAX1674-MAX1676.pdf, accessed Oct. 9, 2015.
[37] A. Nadeau, G. Sharma, and T. Soyata, "State-of-charge estimation for supercapacitors: A Kalman filtering formulation," in *Proc. IEEE ICASSP*, Florence, Italy, May 2014, pp. 2194–2198.
[38] Libelium Waspmote. [Online]. Available: www.libelium.com/products/waspmote/, accessed Aug. 12, 2015.
[39] D. Hooper, J. Coughlan, and M. R. Mullen, "Structural equation modeling: Guidelines for determining model fit," *Electron. J. Bus. Res. Methods*, vol. 6, no. 1, pp. 1–12, Apr. 2008.
[40] H. Elsawy, E. Hossain, and M. Haenggi, "Stochastic geometry for modeling, analysis, and design of multi-tier and cognitive cellular wireless networks: A survey," *IEEE Commun. Surveys Tuts.*, vol. 15, no. 3, pp. 996–1019, Jun. 2013.

DEEPAK MISHRA (S'13) received the B.Tech. degree in electronics and communication engineering from Guru Gobind Singh Indraprastha University, Delhi, India, in 2012. He is currently pursuing the Ph.D. degree with the Department of Electrical Engineering, IIT Delhi, India. His research interests include RF energy harvesting cooperative communication networks and energy optimization schemes for uninterrupted operation of mobile ad hoc networks.

SWADES DE (S'02–M'04–SM'14) received the Ph.D. degree from the State University of New York at Buffalo, NY, USA, in 2004. In 2004, he was an ERCIM Researcher with ISTI-CNR, Italy. From 2004 to 2006, he was with NJIT as an Assistant Professor. He is currently an Associate Professor with the Department of Electrical Engineering, IIT Delhi, India. His research interests include performance study, resource efficiency in wireless networks, broadband wireless access, and optical communication systems.